Influences of ballast degradation on railway track buckling

Ngamkhanong, Chayut; Kaewunruen, Sakdirat; Baniotopoulos, Charalampos

DOI:
10.1016/j.engfailanal.2021.105252

Influences of Ballast Degradation on Railway Track Buckling

Chayut Ngamkhanong[1,2], Sakdirat Kaewunruen[1,2*], Charalampos Baniotopoulos[2]

[1]Department of Civil Engineering, School of Engineering, University of Birmingham, Birmingham B15 2TT, United Kingdom
cxn649@bham.ac.uk; s.kaewunruen@bham.ac.uk; c.baniotopoulos@bham.ac.uk

[2]Birmingham Centre for Railway Research and Education, School of Engineering, University of Birmingham, Birmingham B15 2TT, United Kingdom

Corresponding author
s.kaewunruen@bham.ac.uk

Abstract

Presently, railway track buckling, caused by extreme heat, is a serious issue that causes a huge loss of assets in railway systems. The increase in rail temperature can induce a compression force in the continuous welded rail (CWR) and this may cause track buckling when the compression force reaches the buckling strength. It is important to ensure the lateral stability of railway track in order to tackle the extreme temperature. However, in fact, railway track can be progressively degraded over time resulting in poorer track stability. This includes the larger lateral track misalignment and component deteriorations. This unprecedented study highlights 3D Finite Element Modelling (FEM) of ballasted railway tracks subjected to temperature change considering different ballast fouling conditions. The buckling analysis of ballasted railway tracks considering ballast fouling conditions has been investigated previously. This paper adopts the lateral resistance obtained from the previous single sleeper (tie) push test simulations to the lateral spring model. The influences of the boundary conditions and rail misalignment on the buckling temperature are also investigated. The results clearly show that the ballast fouling may increase the likelihood of track buckling even if the fouled ballast is accumulated at the bottom of the ballast layer. More importantly, the allowable temperature can be reduced up to 50% when the ballast is completely fouled. The results can be used to predict the buckling temperature and to inspect the conditions of ballast. The new findings highlight the buckling phenomena of interspersed railway tracks and help improve the inspection regime of ballast conditions especially in summer to encounter the extreme heat.

Keywords: Railway track buckling, ballast degradation, ballast fouling, snap-through buckling, progressive buckling.

1 Introduction

Railway track buckling is one of the serious issues in the railway system [1-3]. Hence, railway infrastructure developments related to adaptation to future heatwave are expected. In railways, high temperature can possibly induce rail buckling, catenary dilatation, signalling and the heating of rolling stock components. As for railway tracks, the summer heat can significantly increase the rail temperature and cause the rail to expand, leading to a build-up of axial compression force in continuous welded rail (CWR). Although CWR provides a smooth ride and has a lower maintenance cost, it still suffers from drawbacks as the track tends to be buckled easily when the rail temperature reaches a certain limit [4-7]. Based on the evidence [8-10], track buckling can cause derailment and cause a huge loss of assets and can also result in the loss of passenger lives. It is noted that track buckling around the world usually occurs in conventional railway ballasted tracks due to the poor track conditions and lateral misalignment in the rails. Buckling analysis has been widely performed considering sensitivity analysis of major parameters affecting buckling strength [11-16]. Previous studies show that lateral resistance plays the most significant role in buckling strength [17]. The lateral resistance, that can be used properly in buckling analysis, should be obtained from Single Sleeper (Tie) Push Test (STPT) [17-19]. This method provides the ballast-sleeper contact force encountering sleeper movement which can be represented as a track lateral resistance. The lateral force-displacement obtained from STPT can be used as an input for lateral spring element connected to sleeper ends for buckling analysis. As seen in many studies on lateral resistance of ballasted tracks, the displacement limit of the lateral force-displacement obtained by STPTs is usually lower than that those used in buckling analysis. This implies that previous studies have slightly overestimated the buckling temperature of ballasted track.

In fact, railway track is progressively degraded with usage making the improvement of ballasted track necessary, especially at the areas prone to impact loading e.g., short-pitch rail defects, rail joints, coupled defects, crossings [20, 21]. Most importantly, a lack of ballast support can significantly reduce the capacity of railway tracks [22, 23]. For instance, in a track with poor condition, large voids and gaps can easily be observed between sleepers and the ballast, usually caused by the wet track beds (highly moist ground) from natural water springs or poor drainage. The strength and drainage aspects of ballasted tracks are compromised due to the increasing level of ballast fouling. This leads to larger particle movement resulting in more severe loss of support conditions. Hence, and the fouling conditions and degraded ballast decrease lateral resistance of ballasted track. However, in some cases, over the time, lateral resistance could be increased due to the better compaction and consolidation of the ballast layer due to the repeated train loads leading to the lesser void in the ballast layer. This particular case with no ballast breakdown and fouling could possibly lead to higher lateral resistance of tracks [24]. The previous study presented the influences of ballast degradation on lateral resistance. The lateral resistance of railway tracks under ballast fouling conditions have been previously analysed in DEM simulations [25]. It was found that lateral resistance is progressively reduced when the ballast is progressively degraded. The lateral force and sleeper displacement curves were obtained. This study adopts the lateral resistance based on realistic behaviour of degraded ballast to the lateral spring to represent the sleeper-ballast lateral resistance to quantify the buckling phenomenon of ballasted tracks.

The advanced three-dimensional finite element modelling of ballasted railway tracks under various ballast conditions exposed to extreme temperature is presented using LS-DYNA and analysed via nonlinear analysis. This paper studies the buckling phenomena based on the assumptions that ballast fouling is accumulated and formed from the ballast base. The conditions of ballast are divided into 4 stages: Clean, 100mm fouled, 200mm fouled, and completely fouled. The effects of unconstrained length representing the area of degraded ballast in the longitudinal direction are taken into account together with the lateral misalignment of tracks. Note that the buckling temperature derived from different unconstrained lengths can be used to optimise the span number that can potentially be strengthened as a spot replacement. This can also significantly help to minimise the renewal cost of the sleeper at specific spans for increasing the buckling strength instead of increasing the whole track or larger area. This paper thus provides the buckling temperature and allowable temperature of railway tracks under different ballast conditions. The insights will help track engineers to improve track buckling mitigation methods for conventional ballasted tracks.

2 Concept of Railway Track Buckling

If rail temperature is over the neutral temperature or stress-free temperature, the compression axial force in the rails builds up. The rail can be buckled when the compression force reaches its limit or buckling resistance. It should be noted that buckling resistance is affected by track and element types and track conditions. The relationship between rail temperature and lateral displacement is typically plotted as seen in Fig 1. It can be seen that there are two types of buckling depending on the post-buckling path: sudden buckling and progressive buckling. In the pre-buckling stage, the rails are exposed to the temperature over neutral temperature and the axial force is linearly increased. As for the sudden buckling (also called "Snap-through"), the track buckles explosively with no external energy after reaching its maximum temperature (upper critical temperature, T_{Bmax}) and becomes unstable in its post-buckling stages. T_{Bmin} represents the lower bound which can buckle the track if sufficient energy is supplied. It can also be defined as a safe temperature since the track cannot buckle if it experiences a temperature below this temperature. Moreover, progressive buckling can occur when the T_{Bmin} cannot be differentiated from T_{Bmax}. In this case, track lateral displacement is gradually increased after buckling and the critical temperature is defined as T_P.

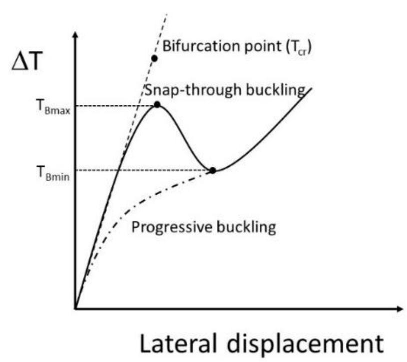

Fig 1. Buckling path.

According to the analytical solutions and buckling shapes observed in the field, there are two main buckling shapes often found: symmetrical and anti-symmetrical shapes. Generally, there are two regions: buckled regions and adjoining regions. The buckled zone is the zone of the change in the shape of the track geometry in the transverse direction, while the rails are deformed longitudinally in the adjoining zone. Fig 2 presents the first symmetrical (Fig 2a) and anti-symmetrical (Fig 2b) shapes and second symmetrical (Fig 2c) and anti-symmetrical (Fig 2d) shapes. The buckled track consists of a buckled region and adjoining region which have a length of l and a, respectively. Subscripts 1 and 2 represent the buckled regions 1 and 2 that the rails are deflected in different shapes. It should be noted that the appropriate nonlinear differential equations governing lateral deflection in the buckled zone and the longitudinal displacement in the adjoining zones are formulated based on large deflection theory [26]. The differential equations are solved to get the resulting equations for different shapes of buckling. For the anti-symmetrical buckling shape, the governing equations are identical to those derived for the symmetrical buckling shape except for the boundary condition. Therefore, the shape of track buckling mostly depends on the boundary conditions which are related to the actual track conditions in the field.

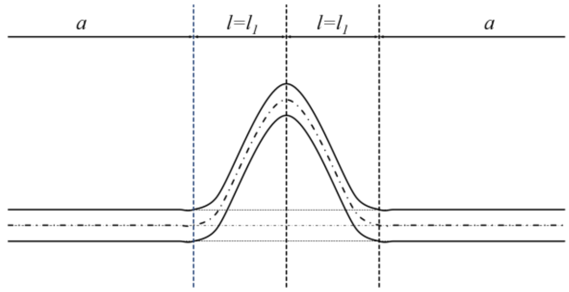

a)

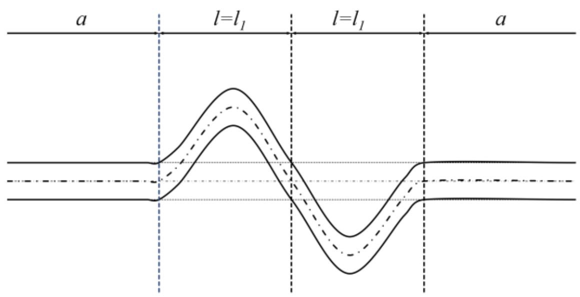

b)

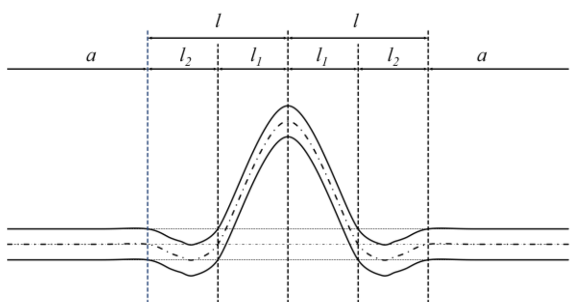

c)

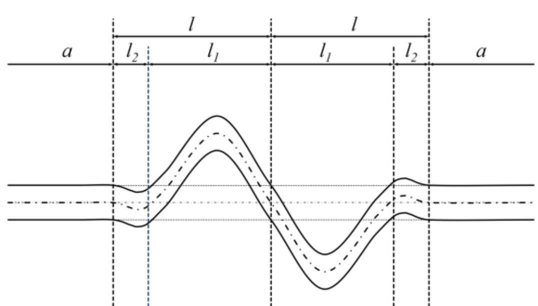

d)

Fig 2. Typical buckling shapes a) symmetrical deformation b) anti-symmetrical deformation c) second symmetrical deformation d) second anti-symmetrical deformation.

3 Ballast Degradation

In general, ballast is progressively fouled over time as the voids among particles are filled with finer materials. The major source of ballast fouling is ballast breakage which is about 76% of all sources. Other sources are infiltration from underlying layers and ballast surface which make up 13% and 7%, respectively. They are followed by subgrade intrusion (3%) and sleeper wear (1%) [27]. It should be noted that ballast fouling greatly undermines the stability and strength of the railway track as mentioned by many researchers [28, 29]. Further, ballast fouling may cause drainage issues in ballasted track since the voids are filled up and water is blocked, leading to higher levels of moisture accumulating in the track substructure [30].

As for ballast fouling mechanism, due to the accumulation of ballast breakdown from load distribution from sleeper or outside contamination, such as subgrade intrusion or coal dust, sand, these finer particles easily fill the voids between particles resulting in undermining track stiffness and shear strength of ballast layer [31-37]. Since more particles are migrated from top to bottom and filled in the voids [38], the ballast particle contacts are eliminated leading to less friction of ballast particles. Those finer materials are accumulated from the bottom and built up all the way to the top until the ballast layer is completely fouled if there is no maintenance and renewal [28, 39]. This study considers the progressive ballast fouling conditions which can be divided into three different levels: 100mm fouled layer, 200mm fouled layer and fully fouled layer. The schematic views of different ballast layer conditions are visualised in Fig 3. In [25], the fouled ballast layer is represented by adding the coal dust in the fouled layer in the simplified DEM simulations. It should be noted that coal dust is represented as a finer material or fouling agent filling in the voids to represent the fouling conditions of the ballast layer. The coal dust acts as a lubricant which can reduce the friction between particles and assigning a lower surface friction angle between two discrete ballast particles/elements in contact is adopted herein for DEM simulations [25].

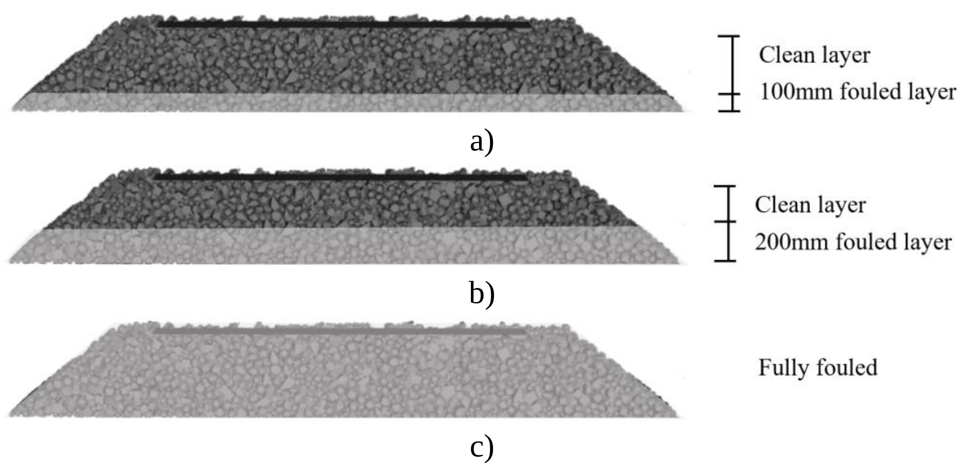

Fig 3. Ballast fouling conditions a) 100mm fouled layer b) 200mm fouled layer c) fully fouled.

4 Methodology

4.1 Finite Element Modelling

In this study, ballasted railway tracks with standard gauge are modelled in LS-DYNA. UIC60 steel rails (A = 76.70 cm^2, Mass = 80.21 kg/m, I_{xx} = 3038.3 cm^4 and I_{yy} = 512.3 cm^4) and mono-block concrete sleepers are modelled as beam elements, which take into account shear and flexural deformations [40]. Rails and sleepers are constructed using SECTION_BEAM and MAT_ELASTIC keywords in LS-DYNA. The MAT_ADD_THERMAL_EXPANSION keyword is assigned to the steel rails to represent the thermal expansion property. The steel rails are connected to the concrete sleepers through the fastener and rail pad which are modelled as the series of spring elements. The rail pads and fasteners are modelled using SECTION_DISCRETE and SPRING_ELASTIC in the connections between the sleepers and the rails. At the rail seat, a rail pad and a fastener, consisting of three translational springs to represent the pad stiffness in three directions and one rotational spring to represent the fastener resistance, are applied. For ballast, the tensionless support spring is considered using user-defined spring property since it allows the beam to life and move over the support while the tensile support is neglected [14]. This presents the realistic behaviour of ballast. The lateral spring of ballast is connected to sleeper ends while the vertical and longitudinal springs are connected to sleepers at rail seats. Note that the simplified lateral springs take into account the contact points between sleeper and ballast along the sleeper length that have been simulated in DEM simulations [25]. The material properties of the ballasted track are presented in Table 1. For track buckling analysis, 60m long ballasted railway tracks are modelled to analyse the effects of the temperature rise on the track. It should be noted that 60m is long enough to capture track buckling phenomena and covers the buckling length observed in practice. The finite element modelling of ballasted tracks with the components is presented in Fig 4a.

Table 1 Material properties.

Parameter list	**Characteristic value**	**Unit**
Rail (UIC60)		
Modulus	2×10^5	MPa
Density	7850	kg/m^3
Poisson's ratio	0.25	
Thermal expansion	1.17×10^{-5}	1/°C
Mono-block concrete sleeper [260x235x2600mm]		
Modulus	3.75×10^4	MPa
Shear modulus	1.09×10^4	MPa
Density	2740	kg/m3
Poisson's ratio	0.2	
Torsional fastening resistance	75	kNm/rad

The lateral spring properties are derived based on the previous STPT simulations using DEM [25]. The lateral spring is applied at sleeper end to represent the whole ballast-sleeper interaction in lateral plane previous obtained by DEM simulations as shown in Fig 4b. It is noted that this spring is the major factor to encounter the sleeper movement in the lateral plane. In DEM, the models were constructed with mono-block concrete sleeper sit on the ballast layer. The ballast layer is simplified as 30mm thick with 400mm wide ballast shoulders and a 1:1.5 shoulder slope. The ballast particles were generated on the basis of the particle distribution curve which conforms to the American Railway Engineering and Maintenance-of-Way Association (AREMA) No. 24 standard specification. The study used coal dust as a fouling agent acting as a lubricant, which can reduce the friction between particles, in the DEM simulations by adapting DEM parameters for different fouling conditions. The actual lateral resistance curves obtained previously are then fit with bilinear curves to be applied to the lateral spring connected at the sleeper ends. The lateral resistance curves and equations used in this study are presented in Fig 5.

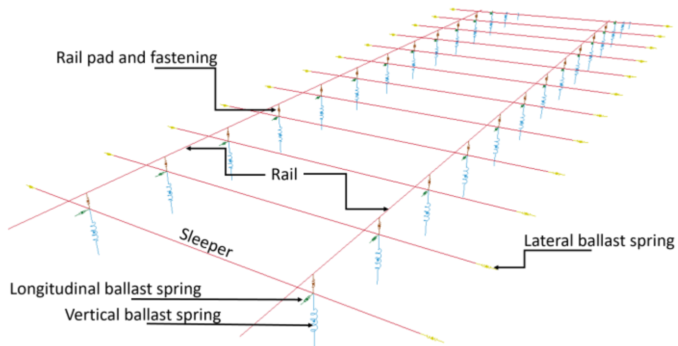

a)

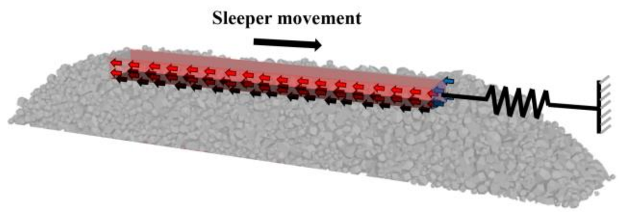

b)

Fig 4. a) Simplified finite element modelling of ballasted railway track b) Lateral ballast spring representing sleeper-ballast lateral resistance.

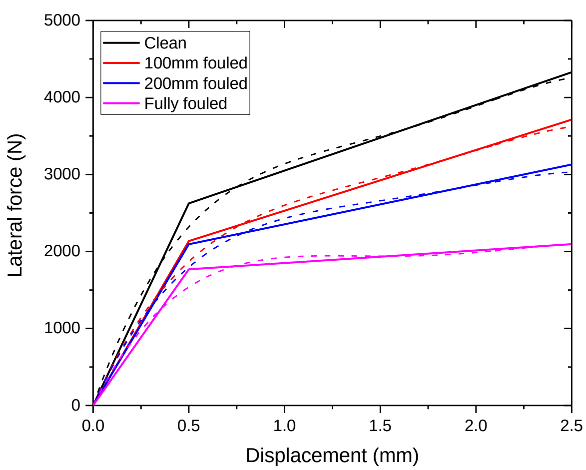

Case	Equation
Clean	*x<0.0005: y = 5264000x* *x≥0.0005: y = 2197+852224x*
100mm fouled	*x<0.0005: y = 4270000x* *x≥0.0005: y = 1740+788404x*
200mm fouled	*x<0.0005: y = 4184000x* *x≥0.0005: y = 1834+517878x*
Fully fouled	*x<0.0005: y = 3538000x* *x≥0.0005: y = 1687+163138x*

y = lateral force (N), x = lateral displacement of sleeper (m)

Fig 5. Lateral force-displacement curve for ballast lateral spring sleepers.

4.2 Boundary Condition

In actual track, there are two regions in the buckled track: buckled regions (positive and negative lateral displacement) and adjoining regions. Due to the extreme temperature, the large lateral displacement of rails normally occurs in a transverse direction if the tracks have imperfections, and the rails are deformed longitudinally in the adjoining region. It is noted that the buckling shapes of a track are often in symmetrical or anti-symmetrical shapes. Note that, the buckling shape and buckling length in the actual track can be changed due to the different track conditions. It is important to note that the buckled region is normally in a weaker zone of the track. The fixed end supports are applied to the end nodes of the rails. The roller supports are applied on the rails to generate the stiff track area so that the rails are constrained and not allowed to move transversally. Hence, the unconstrained length is presented as weaker track and thus this area is expected to buckle. In this study, the track is originally made of 60m length and sufficient for track buckling analysis. As widely observed in the field and analytical solution, buckling length of the first fundamental mode is normally less than 30m, so the largest unconstrained length of 30m is chosen, while beyond this length is considered as the adjoining zone [26]. Meanwhile, tracks buckled with sinusoidal shapes can be seen when the unconstrained length is much larger than that observed in the first few fundamental modes. This is because the buckling length and its shape depend on initial shape of misalignment, the lateral resistance, track stiffness inconsistency which can be defined by the unconstrained length [14]. The boundary conditions of track models are presented in Fig 6. In this study, the unconstrained length starts from 6m and is increased to 12m, 18m, 24m, and 30m, respectively.

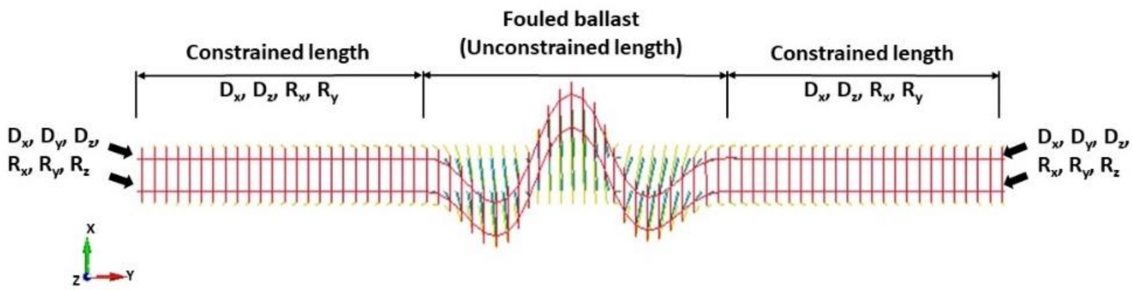

Fig 6. Boundary conditions.

4.3 Nonlinear analysis

To analyse the buckling regime of ballasted tracks, this study uses nonlinear with BGFS quasi newton algorithm in LS-DYNA. This iterative method is for solving unconstrained nonlinear optimisation problems. This approach can produce more accurate results than linear analysis since it includes the nonlinearities and covers both pre- and post-buckling of a structure. However, it has been studied that structure without imperfections cannot be buckled theoretically. It should be noted that perfectly straight tracks remain straight even if they are exposed to extreme temperature and should theoretically buckle. Hence, the initial track imperfection needs to be applied to generate the initial lateral follower force in the rails. It should be noted that initial misalignments are usually seen in the field because of the incorrect stress adjustment, loss of track geometry, loss of lateral resistance etc. This can trigger the lateral force in rails leading to larger misalignment and possible track buckling. The shape of initial misalignment is based on fundamental buckling shape that has been previously analysed using eigenvalue analysis [14]. It should be noted that the allowable misalignment can be up to over 30mm depending on the class of track [41, 42]. Thus, the initial misalignments of between 8 and 32m are applied on the rails at mid-tracks.

It is noted that, based on previous STPTs on ballast lateral resistance, the load-displacement curves are likely to be bi-linear. The lateral resistance curves obtained in Fig 5 are applied using user-defined CURVE_DEFINED keyword. These curves are then linked to the lateral spring in keyword MAT_SPRING_INELASTIC with the consideration of tension only. The temperature of 200 °C is applied to the system using the keyword LOAD_THERMAL_LOAD_CURVE in LS-DYNA. The thermal expansion is applied to the rails using the keyword MAT_ADD_THERMAL_EXPANSION. The following parameters also are considered.

- Lateral ballast resistance considering 4 scenarios: Clean ballast, 100mm fouled ballast, 200mm fouled and fully fouled ballast.
- Fouling area of ballast represented by unconstrained length: 6-30m
- Initial track misalignment (imperfection): 8-32mm.

4.4 Model validation

Due to limitations in buckling test in both laboratory and field that are difficult and have never been conducted, the preliminary results should be validated with previous analytical solution and finite element modelling. It should be noted that the parameters used for each track components have been validated using experimental parameters, field data, and previous laboratory results [43, 44]. Those parameters are combined to build up the ballasted track. The straight ballasted track is considered for model validation. This track consists of UIC60 steel rails sat on concrete sleepers. The initial lateral stiffness of 200N/mm and fastener torsional stiffness of 75kNm/rad are considered to compare with the previous studies as these values represent similar track conditions and properties with previous studies. The result is validated against two different previous analytical solutions and FEM results. The analytical solutions are based on the principle of the virtual displacement equation and bending beam theory. The results are solved by assuming the buckling shape and applying the chosen track parameters to the equation. The buckling temperature is then calculated from the corresponding value of axial force [45, 46]. The previous finite element approach in ANSYS used an indirect method combining two rails into one idealised continuous beam with four springs representing the ballast and fastening with a spacing of 1m along the beam [47]. The objective of the indirect method was to evaluate the safe temperature by analysing various progressive buckling modes with a similar lateral resistance force of ballast. As the buckling modes in those studies were expected to be progressive buckling mode, linear buckling analysis can potentially obtain the safe temperature directly from the eigenvalue. The model of ballasted tracks constructed in another FEM software, STRAND7, is also compared to the current model in this study [14]. The method used was linear eigenvalue analysis and thus only the buckling temperature was obtained. Table 2 presents a comparison between previous studies and the preliminary result from the current model. Note that the buckling progressive failure mode is obtained so that the safe temperature can be presented as the buckling temperature. It is found that the result obtained in this study is within the acceptable range of previous studies as the percentage difference of buckling temperature of example model is less than 5% and thus the models can be used appropriately.

Table 2 Buckling temperatures for model validation (°C).

Case	Analytical solutions		FEM		Average	This study	Difference (%)
	[45]	[46]	[47]	[14]			
Torsional resistance = 75 kNm/rad	57.7	47.8	50.0	53.0	52.1	54.1	3.7

5 Results and Discussions

5.1 Buckling temperature

Fig 7 presents the buckling temperature over neutral and rail axial force considering the influences of ballast degradation. The effects of unconstrained length are also compared. It is observed that railway tracks are generally buckled within the same ranges when the track has an unconstrained length larger than 18 whereas railway tracks with 6m and 12m are buckled with much higher temperature. Larger initial track misalignments yield a lower buckling temperature. As for the track with unconstrained lengths of 6m and 12m, the buckling temperature for all ballast conditions has different trends depending on the initial misalignment amplitude. The buckling temperature of railway tracks with an unconstrained length of 12m tends to be smaller when the initial misalignment becomes larger. Moreover, ballast degradation has a significant effect in reducing buckling temperature especially when the ballast is fully fouled. While the buckling temperatures of railway tracks with partially fouled ballast are lower than those with clean ballast, however, railway tracks with 100mm and 200mm fouled ballast yields within the close buckling temperature. This is due to the fact that the fouled ballast is located at the bottom layer which is not directly contacted to the sleeper bottom leading to the close trend in lateral resistance.

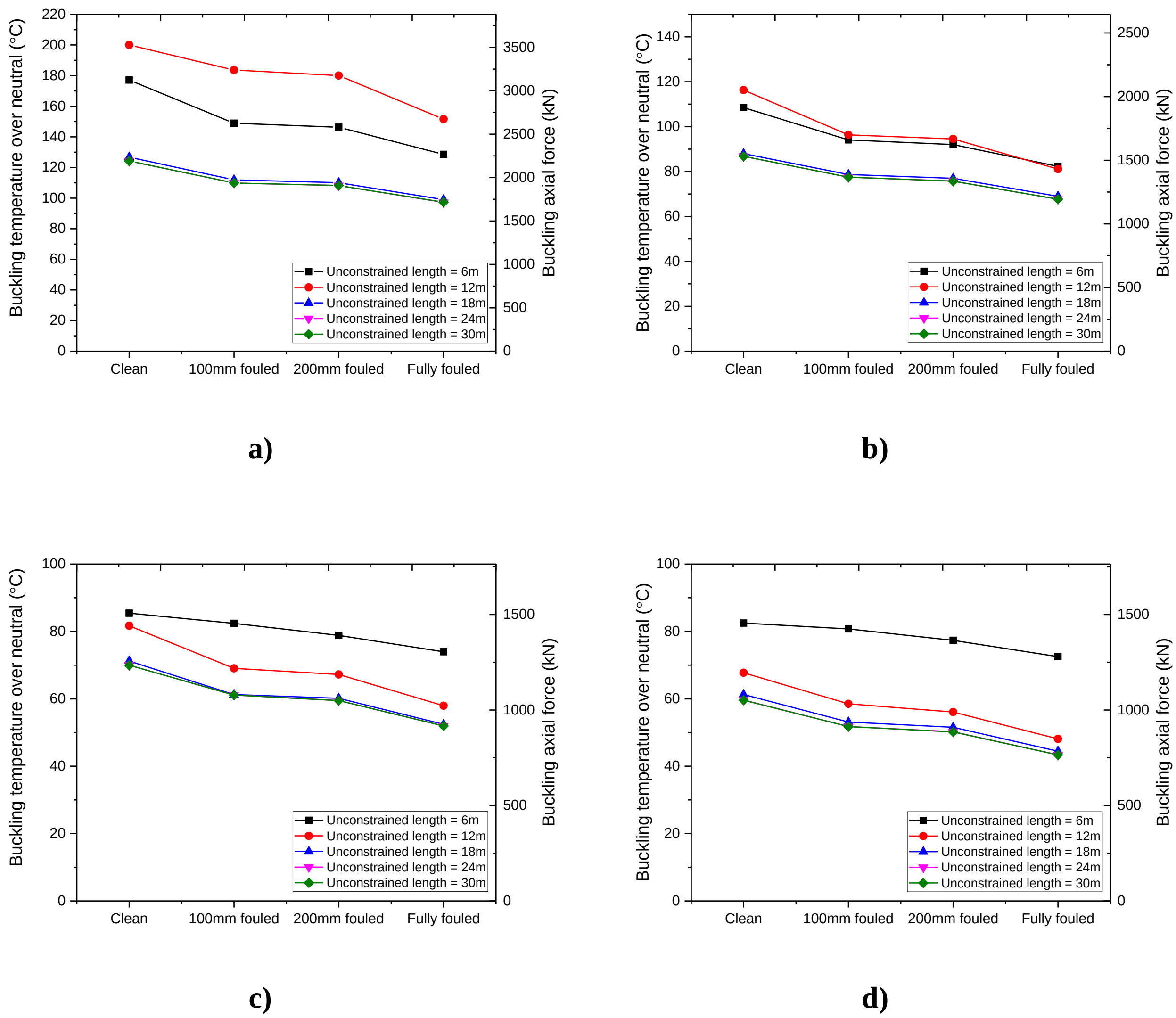

Fig 7. Buckling temperature over neutral and buckling axial force a) misalignment = 8m b) misalignment = 16m c) misalignment = 24m d) misalignment = 32m.

5.2 Rail axial force

As for safe temperature, it can be calculated in the post-buckling stage. If the snap-through buckling occurs, the axial force is dropped immediately after buckling and the track falls into the unstable stage until it reaches the level where the track excites and tends to be constant in the post-buckling stage. After a certain level, railway track becomes stable and the expansion of lateral displacement is due to the lateral resistance. It is noted that a safe temperature can be predictable and calculated by drawing the trend line of the axial force in the post-buckling stage. This can be drawn backwards until this line intersects with the rail axial force in the pre-buckling stage. The projection of this intersection point is the rail axial force that might buckle the track at minimum or safe temperature. Whereas the axial force of progressive buckling track is not suddenly dropped but progressively so that the safe temperature cannot be seen as in snap-through buckling.

Fig 8 presents the rail axial force against the increase in rail temperature of railway tracks with clean ballast. This figure compares axial force of rail in railway tracks with misalignment amplitude between 8mm and 32mm. As for track with 6m unconstrained length, the buckling mode can be either progressive or snap-through depending on the misalignment amplitude. When railway tracks have low misalignment (8mm and 16mm), buckling mode is likely to be progressive while the snap-through can be observed when the track has 24mm and 32mm misalignments. Whereas railway tracks with larger unconstraint length (Fig 8b), track buckling tends to be in snap-through buckling failure. It is noted that rail axial forces for all cases are likely to be the same once the tracks become stable.

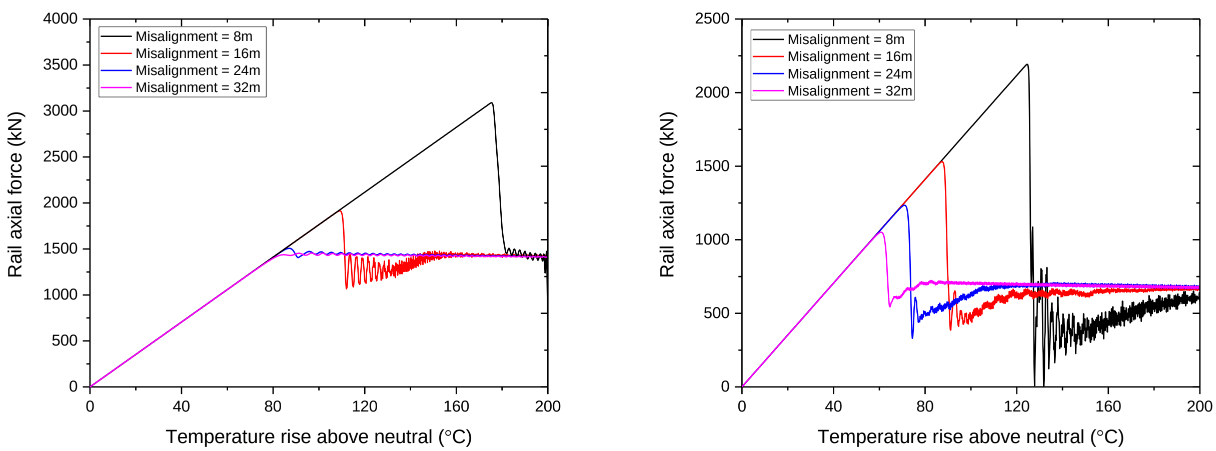

a) **b)**

Fig 8. Rail axial force – temperature rise above neutral of tracks with clean ballast and a) 6m unconstrained length b) 30m unconstrained length.

Fig 9 compares the rail axial force – temperature rise between unconstrained lengths considering ballast fouling conditions. It is clear that the ballast fouling has a significant influence in buckling temperature reduction for all cases especially when the ballast is fully fouled due to the reduction of axial buckling force. Safe temperature is also significantly reduced when the ballast is fully fouled, however, the safe temperature is not affected much when 100mm fouled ballast thickness is considered. Moreover, rail excitations in the post-buckling stage are not observed when the misalignment is large while it is seen when 8mm misalignment is considered especially when the unconstrained length of railway tracks is 30m (Fig 9d),

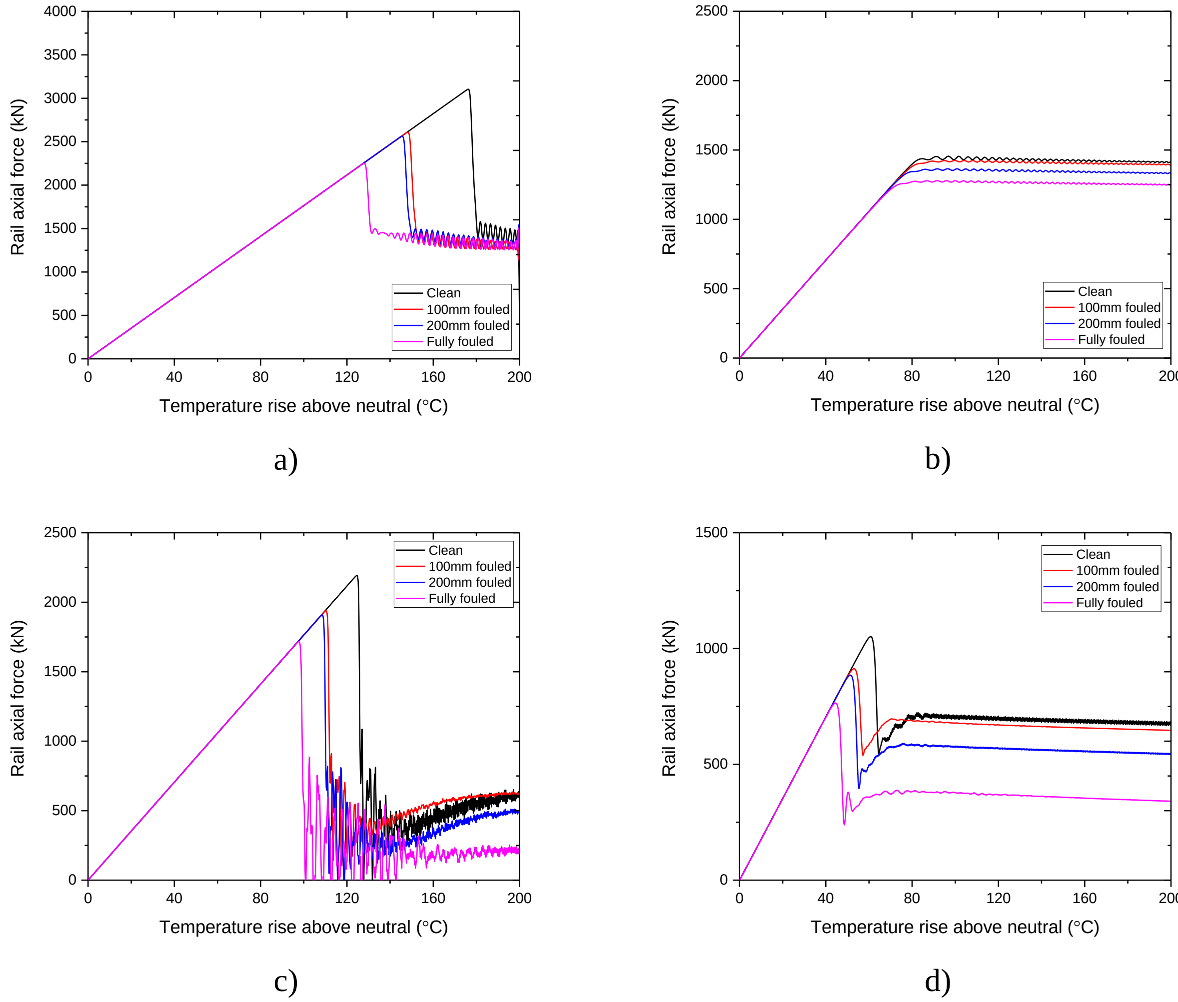

Fig 9. Rail axial force – temperature rise above neutral of tracks considering ballast fouling conditions a) 6m unconstrained length, 8mm misalignment b) 6m unconstrained length, 32mm misalignment c) 30m unconstrained length, 8mm misalignment d) 30m unconstrained length, 32mm misalignment.

Both buckling and safe temperatures are plotted in Fig 10. The effects of both misalignment and ballast conditions are considered. Overall, the ballast fouling conditions have significant effects on buckling temperature reduction. It should be noted that buckling temperature is crossed or in contact with the safe temperature curve when the progressive buckling occurs. This phenomenon can be seen in Fig 10a at the misalignment amplitudes of 24mm and 32 while the buckling temperature and safe temperature are distinctly separated in other cases resulting in snap-through failure. Again, it is clear from this figure that safe temperature is not affected by misalignment amplitude. Moreover, reducing unconstrained length is likely to increase the buckling temperature. However, it is also remarkable that the buckling temperature of tracks with 12m unconstrained length is larger than those of tracks with 6m unconstrained length. This is because of the effects of unconstrained length on the misalignment curves showing that the track with 6-m unconstrained length tends to be the curved track that can largely reduce track stability and buckling temperature. This implies that the further use of the outcome of the unconstrained length for spot replacement method should be proposed on the straight track to maximise the benefit of the spot replacement method.

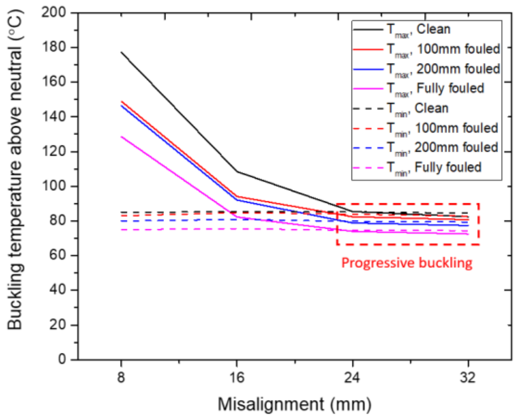

a) 6m

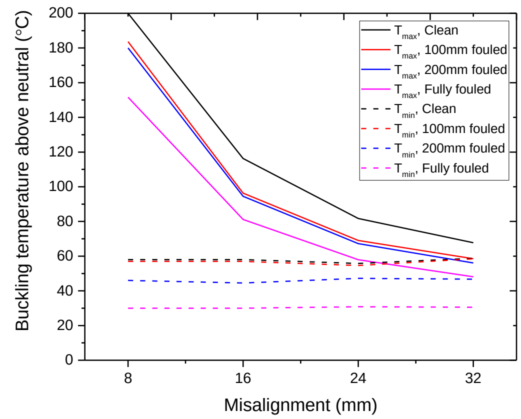

b) 12m

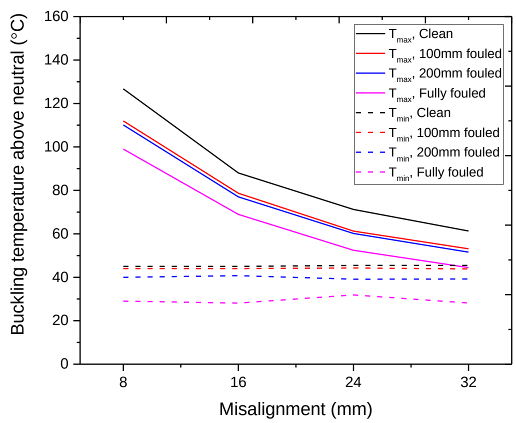

c) 18m

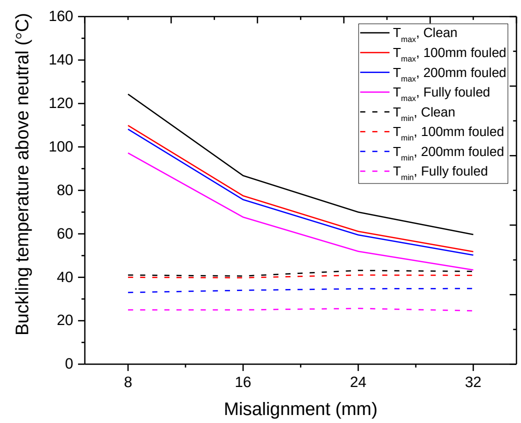

d) 24m

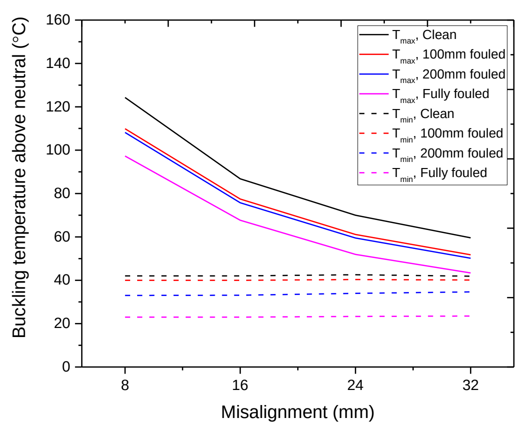

e) 30m

Fig 10. Buckling temperature and safe temperature a) unconstrained length = 6m b) unconstrained length = 12m c) unconstrained length = 18m d) unconstrained length = 24m e) unconstrained length = 30m

5.3 Safety criteria

Safety criteria of railway track buckling have been determined from the difference between buckling temperature and safe temperature [48]. The allowable temperature above neutral (T_{all}), where the rail has zero stress, can be evaluated as shown in Table 3. The allowable temperature is generally calculated from safe temperature. It should be noted that the difference in buckling criteria depends on ΔT or buckling failure modes. The allowable temperature of progressive buckling track, which falls in the last criterion, is generally lower than the that of snap-through buckling failure. This implies that tracks should not be in the conditions which can possibly buckle the track progressively.

Table 3 Safety criteria and allowable temperature [48]

Criteria	Allowable temperature (°C)
$\Delta T > 20°C$	$T_{all} = T_{min} + 0.25\Delta T$
$5°C \leq \Delta T \leq 20°C$	$T_{all} = T_{min}$
$0°C \leq \Delta T < 5°C$	$T_{all} = T_{min} - 5$

Where $\Delta T = T_{max} - T_{min}$

Fig 11 presents the allowable temperature rise over neutral. It is calculated based on the safety criteria presented in Table 3. It is clearly seen that fouled ballast can significantly reduce the allowable temperature which increases the likelihood of track buckling. This can also be seen in Fig 10 that T_{max} and T_{min} are quite close whereas increasing the possibility of progressive buckling failure. For this reason, the allowable temperature is significantly low in comparison to railway tracks with a better condition where snap-through buckling can occur. Moreover, fouled ballast that occurs in the larger area coupled with track larger misalignment greatly reduce the allowable temperature. The allowable temperature can be lower than 30 °C which can be observed in reality.

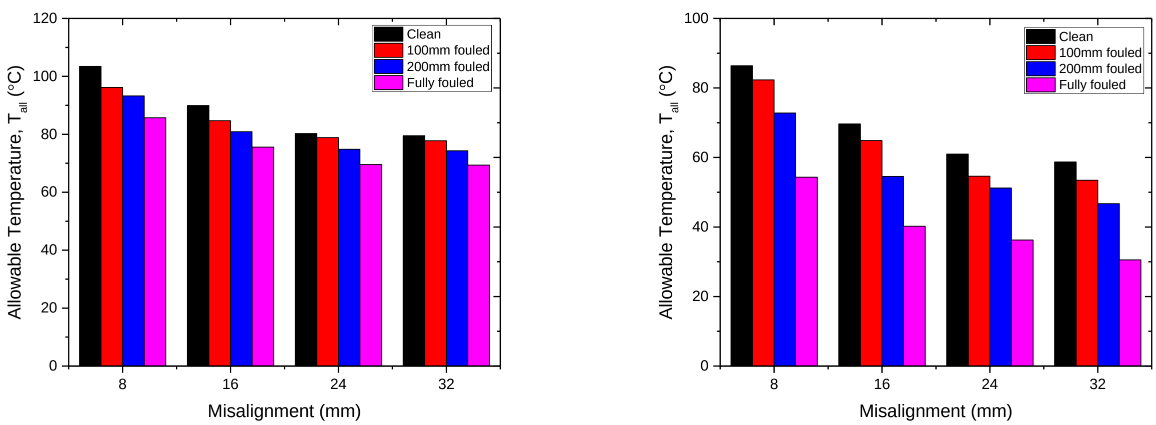

a) b)

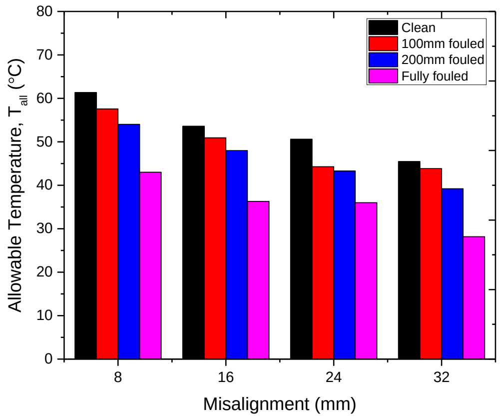

c)

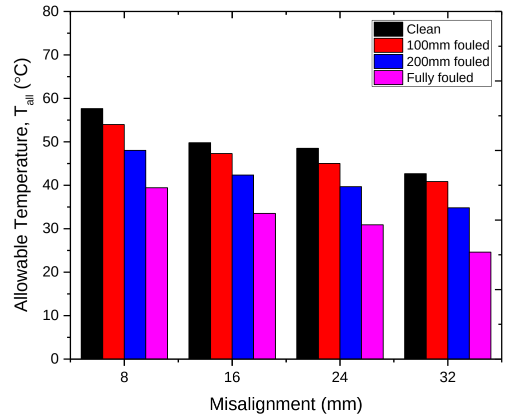

d)

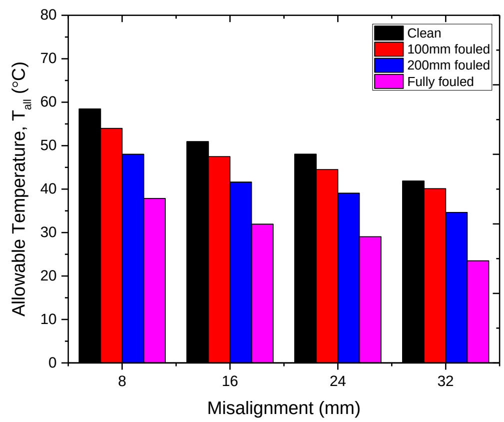

e)

Fig 11. Allowable temperature rise of railway tracks a) unconstrained length = 6m b) unconstrained length = 12m c) unconstrained length = 18m d) unconstrained length = 24m e) unconstrained length = 30m.

6 Conclusions

In this study, 3D finite element models are developed to investigate the buckling behaviour of ballasted railway tracks considering ballast degradation. Three cases of ballast fouling conditions are considered in this study. The lateral resistance curves obtained from previous simplified DEM simulations at different ballast conditions are applied as an input for ballast lateral spring in track buckling modelling. The key findings are revealed by the obtained results as follows.

- Reducing the unconstrained length to 12m or 20 spans can potentially reduce the risk of track buckling. This finding can help optimise the proper strengthening method for buckling strength by restraining the sleeper at the optimised spans. The unconstrained length suggests the location of spot replacement that can effectively increase buckling temperature. For instance, restraining the sleeper in a lateral plane every 20 spans by replacing the old ones by the frictional concrete sleeper can significantly increase buckling strength for the whole track not only just one span.
- Generally, snap-through buckling normally occurs especially for the ballasted track with new clean ballast. However, in the same track, buckling failure mode can be shifted from snap-

through to progressive buckling when the track is degraded including poorer track lateral misalignment and ballast fouling conditions.

- The risk of track buckling is far greater for railway tracks with fouled ballast conditions even if the fouled ballast is hidden in the bottom layer where there is no direct contact to the sleeper. This shows that the buckling strength of ballast track is reduced over time due to the progressive degradation of ballast leading to prone to buckling.
- Fouling condition coupled with larger track misalignment can significantly reduce the allowable temperature.
- When the ballast layer is completely fouled, the allowable temperature of rails falls in between 20 °C and 30 °C that can be widely observed in summer. This is clear that track buckling can occur on degraded tracks.

This is confirmed that inspection of ballast is essential even though ballast condition seems to be good by visual inspection as the hidden degraded ballast at the bottom layer can still undermine the buckling strength resulting in increasing risk of track buckling. It is obvious that ballast fouling can result in a significant reduction of the buckling strength. Hence, it is important to reduce the stress on ballast to prevent ballast breakage and maintain the stability of railway tracks, especially at the areas prone to impact loading, e.g. rail joints, dipped rails, crossing, misaligned tracks. The insights will enhance the inspection of ballast conditions in railway systems and mitigate the risk of delays due to unplanned maintenance, thus paving a robust pathway for a practical impact on societies.

7 Acknowledgements

The authors are sincerely grateful to European Commission for the financial sponsorship of the H2020-MSCA-RISE Project No. 691135 “RISEN: Rail Infrastructure Systems Engineering Network,” which enables a global research network that tackles the grand challenge of railway infrastructure resilience and advanced sensing in extreme environments (www.risen2rail.eu) [49]. Some research work has been carried out by the first author during his RISEN secondment (visiting student) at the Department of Civil and Environmental Engineering, the University of Illinois at Urbana-Champaign, USA. The first would like to express his sincere appreciation to Prof Erol Tutumluer and Prof Youssef M A Hashash from the University of Illinois at Urbana-Champaign for the valuable comments and support during his stay in the USA.

8 Reference

1. I. S. Oslakovic, H. W. T. Maat, A. Hartmann, G. Dewulf, Risk Assessment of Climate Change Impacts on Railway Infrastructure, **(2013)**.
2. A. D. Quinn, A. Jack, S. Hodgkinson, E. J. S. Ferranti, J. Beckford, J. Dora, Rail Adapt: Adapting the Railway for the Future, A Report for the International Union of Railways (UIC) **(2017)**.
3. C. Ngamkhanong, S. Kaewunruen, B. J. A. Costa, State-of-the-Art Review of Railway Track Resilience Monitoring, Infrastructures. 3(1) **(2018)** 3.
4. S. S. N. Ahmad, N. K. Mandal, G. Chattopadhyay. "A Comparative Study of Track Buckling Parameters on Continuous Welded Rail." 26-28.
5. C. Esveld, *Modern Railway Track*. Vol. 385: MRT-productions Zaltbommel, Netherlands, 2001.

6. A. Kish, On the Fundamentals of Track Lateral Resistance, American Railway Engineering and Maintenance of Way Association (**2011)**.

7. C. Esveld. "Improved Knowledge of Cwr Track." 8-9, 1997.

8. L. Ling, X. B. Xiao, Y. B. Cao, L. Wu, Z. Wen, X. S. Jin, Numerical Simulation of Dynamical Derailment of High-Speed Train Using a 3d Train–Track Model. 2014.

9. L. Ling, X. B. Xiao, X. S. Jin, Development of a Simulation Model for Dynamic Derailment Analysis of High-Speed Trains, Acta Mechanica Sinica. 30(6) (**2014)** 860-75.

10. S. Kaewunruen, Y. Wang, C. Ngamkhanong, Derailment-Resistant Performance of Modular Composite Rail Track Slabs, Engineering Structures. 160 (**2018)** 1-11.

11. M. Cuadrado, C. Zamorano, P. González, J. Nasarre, E. Romo, Analysis of Buckling in Dual-Gauge Tracks, Proceedings of the Institution of Civil Engineers-Transport. 161 (**2008)** 177-84.

12. I. Villalba, R. Insa, P. Salvador, P. Martinez, Methodology for Evaluating Thermal Track Buckling in Dual Gauge Tracks with Continuous Welded Rail, Proceedings of the Institution of Mechanical Engineers, Part F: Journal of Rail and Rapid Transit. 231(3) (**2017)** 269-79.

13. G. Yang, M. A. Bradford, Thermal-Induced Buckling and Postbuckling Analysis of Continuous Railway Tracks, International Journal of Solids and Structures. 97 (**2016)** 637-49.

14. C. Ngamkhanong, C. M. Wey, S. Kaewunruen, Buckling Analysis of Interspersed Railway Tracks, Appl. Sci. 10 (**2020)** 3091.

15. P. Liu, B.-J. Tang, S. Kaewunruen, Vibration-Induced Pressures on a Cylindrical Structure Surface in Compressible Fluid, Applied Sciences. 9(7) (**2019)** 1403.

16. P. Liu, S. Kaewunruen, B.-j. Tang, Dynamic Pressure Analysis of Hemispherical Shell Vibrating in Unbounded Compressible Fluid, Applied Sciences. 8(10) (**2018)** 1938.

17. G. Jing, P. Aela, Review of the Lateral Resistance of Ballasted Tracks, Proceedings of the Institution of Mechanical Engineers, Part F: Journal of Rail and Rapid Transit. 234(8) (**2020)** 807-20.

18. A. Kish. "On the Fundamentals of Track Lateral Resistance." In *Annual Conference*. Minneapolis, USA, 2011.

19. Y. Guo, H. Fu, Y. Qian, V. Markine, G. Jing, Effect of Sleeper Bottom Texture on Lateral Resistance with Discrete Element Modelling, Construction and Building Materials. 250 (**2020)**.

20. C. Ngamkhanong, S. Kaewunruen, Effects of under Sleeper Pads on Dynamic Responses of Railway Prestressed Concrete Sleepers Subjected to High Intensity Impact Loads, Engineering Structures. 214 (**2020)**.

21. S. Kaewunruen, C. Chiengson, Railway Track Inspection and Maintenance Priorities Due to Dynamic Coupling Effects of Dipped Rails and Differential Track Settlements, Engineering Failure Analysis. 93 (**2018)** 157-71.

22. B. Feng, W. Hou, E. Tutumluer, Implications of Field Loading Patterns on Different Tie Support Conditions Using Discrete Element Modeling: Dynamic Responses, Transportation Research Record: Journal of the Transportation Research Board. 2673(2) (**2019)** 509-20.

23. W. Hou, B. Feng, W. Li, E. Tutumluer, Evaluation of Ballast Behavior under Different Tie Support Conditions Using Discrete Element Modeling, Transportation Research Record: Journal of the Transportation Research Board. 2672(10) (**2018)** 106-15.

24. A. Kish, G. Samavedam. "Track Buckling Prevention: Theory, Safety Concepts, and Applications." John A. Volpe National Transportation Systems Center (US), 2013.

25. C. Ngamkhanong, B. Feng, E. Tutumluer, Y. M. Hashash, S. Kaewunruen, Evaluation of Lateral Stability of Railway Tracks Due to Ballast Degradation, Construction and Building Materials (**2021)**.

26. A. D. Kerr, Analysis of Thermal Track Buckling in the Lateral Plane, Acta Mechanica. 30(1-2) (**1978)** 17-50.

27. E. T. Selig, J. M. Waters, *Track Geotechnology and Substructure Management*. London, UK, 1994.

28. T. R. Sussmann, M. Ruel, S. M. Chrismer, Source of Ballast Fouling and Influence Considerations for Condition Assessment Criteria, Transportation Research Record: Journal of the Transportation Research Board (**2012)** 87-94.

29. N. Tennakoon, B. Indraratna, S. Nimbalkar. "Impact of Ballast Fouling on Rail Tracks." In *International Conference on Railway Technology: Research, Development and Maintenance* Scotland: Civil-Comp Press, 2014.

30. W. O. Danquah, G. S. Ghataora, M. P. N. Burrow. "The Effect of Ballast Fouling on the Hydraulic Conductivity of the Rail Track Substructure." In *XV Danube - European Conference on Geotechnical Engineering (DECGE 2014)*. Vienna, Austria, 2014.

31. A. R. TolouKian, J. Sadeghi, J.-A. Zakeri, Large-Scale Direct Shear Tests on Sand-Contaminated Ballast, Proceedings of the Institution of Civil Engineers - Geotechnical Engineering. 171(5) (**2018)** 451-61.

32. A. R. Tolou Kian, J. Sadeghi, J.-A. Zakeri, Influences of Railway Ballast Sand Contamination on Loading Pattern of Pre-Stressed Concrete Sleeper, Construction and Building Materials. 233 (**2020)** 117324.

33. J. Sadeghi, A. R. Tolou Kian, H. Ghiasinejad, M. Fallah Moqaddam, S. Motevalli, Effectiveness of Geogrid Reinforcement in Improvement of Mechanical Behavior of Sand-Contaminated Ballast, Geotextiles and Geomembranes. 48(6) (**2020)** 768-79.

34. J. Sadeghi, A. R. T. Kian, M. Fallah, Experimental Investigation of Mechanical Properties of Ballast Contaminated with Wet Sand Materials, International Journal of Geomechanics. 21(1) (**2021)** 04020241.

35. A. R. T. Kian, J. A. Zakeri, J. Sadeghi, Experimental Investigation of Effects of Sand Contamination on Strain Modulus of Railway Ballast, Geomechanics and Engineering. 14(6) (**2018)** 563-70.

36. H. Huang, E. Tutumluer, Discrete Element Modeling for Fouled Railroad Ballast, Construction and Building Materials. 25(8) (**2011)** 3306-12.

37. H. Huang, E. Tutumluer, W. Dombrow, Laboratory Characterization of Fouled Railroad Ballast Behavior, Transportation Research Record: Journal of the Transportation Research Board. 2117(1) (**2009)** 93-101.

38. P. Anbazhagan, T. P. Bharatha, G. Amarajeevi, Study of Ballast Fouling in Railway Track Formations, Indian Geotechnical Journal. 42(2) (**2012)** 87-99.

39. Federal Railroad Administration. "Heavy Axle Load Revenue Service Mudfouled Ballast Investigation." In *RESEARCH RESULTS REPORT* U.S. Department of Transportation, 2011.

40. Z. Cai, Modelling of Rail Track Dynamics and Wheel/Rail Interaction. PhD Thesis, Queen’s University, Kingston, ON, Canada, 1994.

41. CRC for Rail Innovation. "Track Stability Management – Literature Review: Theories and Practices ". Brisbane, Australia: CRC for Rail Innovation 2009.

42. Federal Railroad Administration (FRA). "Continuous Welded Rail (Cwr); General." Federal Railroad Administration (FRA), 2010.

43. S. Kaewunruen, T. Lewandrowski, K. Chamniprasart. "Nonlinear Modelling and Analysis of Moving Train Loads on Interspersed Railway Tracks." 15-17, 2018.

44. S. Kaewunruen, C. Ngamkhanong, J. Ng, Influence of Time-Dependent Material Degradation on Life Cycle Serviceability of Interspersed Railway Tracks Due to Moving Train Loads, Engineering Structures. 199 (**2019)** 109625.

45. M. A. Prud'Homme, M. G. Janin, The Stability of Tracks Laid with Long Welded Rails, Rail International. 46 (**1969)** 459-87.

46. A. D. Kerr, An Improved Analysis for Thermal Track Buckling, International Journal of Non-Linear Mechanics. 15(2) (**1980)** 99-114.

47. J. Carvalho, J. Delgado, R. Calcada, R. Delgado, A New Methodology for Evaluating the Safe Temperature in Continuous Welded Rail Tracks, International Journal of Structural Stability and Dynamics. 13(02) (**2013)** 1350016.

48. European Rail Research Institute Committee D202. "Improved Knowledge of Forces in Cwr Track (Including Switchws)." In *Report2, review of existing experimental work in behaviour of CWR track*. Utrecht, Netherlands: European Rail Research Institute 1995.

49. S. Kaewunruen, J. M. Sussman, A. Matsumoto, Grand Challenges in Transportation and Transit Systems, Frontiers in Built Environment. 2(4) (**2016)**.